Nonlinear Dyn (2019) 96:1067–1081
https://doi.org/10.1007/s11071-019-04839-4

ORIGINAL PAPER

Vibration energy harvesting under concurrent base and flow excitations with internal resonance

Haojie Liu · Xiumin Gao

Received: 20 September 2018 / Accepted: 12 February 2019 / Published online: 27 February 2019

Abstract In this study, internal resonance is investigated to further explore the potential of energy harvesting under concurrent base and flow excitations. The effects of system parameters on the performance of energy harvester with three-to-one internal resonance are analyzed analytically. At first, a lumped-parameter model for the energy harvester, which consists of a two-degree-of-freedom airfoil with the piezoelectric coupling introduced to the plunging motion, is established by using a nonlinear quasi-steady aerodynamic model. Subsequently, the method of multiple scales is implemented to derive the approximate analytic solution of the energy harvesting system under three-to-one internal resonance. Then, the bifurcation characteristics of the energy harvester with respect to various system parameters are analyzed. Finally, the numerical solutions are presented to validate the accuracy of the approximate analytic solutions. The study shows that the harvested voltage and power of the energy harvester can be significantly improved in the presence of internal resonance. In addition, the analytic solutions of internal resonance and the bifurcation analysis can provide an essential reference for design of such a kind of energy harvester.

Keywords Internal resonance · Energy harvesting · The method of multiple scales · Analytic solutions · Concurrent excitations

1 Introduction

Energy harvesting technologies harness ambient energy and convert it to electrical energy that can operate small electronic devices [1]. They show great potential for the applications of low-powered electronic devices, especially when battery recharging or replacement is difficult and expensive. There are various energy sources available for energy harvesting, such as wind, solar, thermal energy and vibration energy. Among these energy sources, energy harvesting from base-excited vibration has attracted increasing interests over the past decade [2].

Flow-induced vibrations, that may cause structural fatigue or damage, are usually seen as negative phenomena and need to be suppressed by using passive or active control techniques [3–9]. From the view of energy harvesting, however, flow-induced vibrations can be considered as one of the most promising energy sources due to the self-excited characteristics. Recent years have witnessed increasing interests in exploiting flow-induced vibrations aiming at providing efficient, scalable energy harvesters [10–12]. In general, there are

H. Liu
State Key Laboratory of Mechanics and Control of Mechanical Structures, Nanjing University of Aeronautics and Astronautics, Nanjing, China

X. Gao (✉)
School of Physical and Mathematical Sciences, Nanjing Tech University, Nanjing 210016, People's Republic of China
e-mail: gaoxm@njtech.edu.cn

three flow-induced vibration mechanisms for energy harvesting, namely vortex-induced vibration [13,14], galloping [15,16] and flutter [17–19]. Almost all the aforementioned studies only considered one type of ambient vibration energy source, either base or flow induced. However, these two types of vibration energies are available for some applications like aerospace engineering. Hence, several researchers have exploited the potential of harnessing vibration energy under concurrent base and flow excitations. Bibo and Daqaq [20,21] are among the first to investigate vibration energy harvesting under the combination of base and flow excitations. In their study, a flutter-based energy harvester was subjected to base excitation in the plunging direction. As shown by the results, the output power from base excitations was amplified due to unsteady flow effects when the flow speed is below the flutter speed. On the other hand, the output power from flutter could be decreased or increased relying on the characteristics of base excitation when the flow speed is above the flutter speed. Subsequently, Yan and Abdelkefi [22] proposed a piezoelectric energy harvester to harness vibration energy under concurrent base and galloping excitations. The nonlinear characteristics of the energy harvester were determined by using frequency spectrum, phase diagram and Poincaré sections. Furthermore, Dai et al. [23] proposed a piezoelectric energy harvester to harness vibration energy under concurrent base and vortex-induced vibrations.. It was found that the output power of the energy harvester under combined excitations was significantly improved when the flow speed fell in the lock-in region of the cylinder. Very recently, Zhao and Yang [24] proposed a broadband energy harvester to concurrently harness vibration energy from base and flow excitations. The bandwidth of the energy harvester was broadened by utilizing a mechanical stopper fixed at the bottom of the cantilever.

In this study, internal resonance is investigated to further explore the potential of energy harvester under concurrent base and flow excitations. The effects of system parameters on the performance of energy harvester with three-to-one internal resonance are analyzed analytically. Although internal resonance has attracted many attentions for vibration energy harvesting under base excitations [25–32], to the authors' best knowledge, there are few efforts paid to vibration energy harvesting in the presence of internal resonance under concurrent base and flow excitations. To fill the gap, the present work attempts to explore the possibility of improving energy harvesting performance under concurrent base and flow excitations by introducing the internal resonance. In particular, an energy harvester which consists of a two-degree-of-freedom airfoil is established in the present study. The analytic solutions of internal resonance and the bifurcation characteristics are obtained by using the method of multiple scales.

The remainder of this study is organized as follows. In Sect. 2, the lumped-parameter model of the energy harvester is established under concurrent base and flow excitations. In Sect. 3, the approximate analytic solutions of three-to-one internal resonance are derived via the method of multiple scales. In Sect. 4, the effects of system parameters on the harvested voltage and power are investigated. In Sect. 5, the numerical results are presented to validate the approximate analytic solutions. Finally, some conclusions are drawn in Sect. 6.

2 Piezoaeroelastic system modeling

As shown in Fig. 1, the energy harvester consists of a rigid airfoil with pitching and plunging degrees of freedom and piezoelectric coupling is introduced to the plunging degree of freedom. The governing equations of the harvester under concurrent base and flow excitations can be written as

$$\begin{aligned} &m_T\ddot{h} + m_W x_\alpha b\ddot{\alpha} + c_h\left(\dot{h}-\dot{z}\right) + k_h h - \theta V = -L \\ &m_W x_\alpha b\ddot{h} + I_\alpha\ddot{\alpha} + c_\alpha\dot{\alpha} + k_\alpha\alpha = T \\ &C_p\dot{V} + V/R_l + \theta\left(\dot{h}-\dot{z}\right) = 0 \end{aligned} \tag{1}$$

where h and α are the plunging and pitching displacements of the airfoil. b is the half chord length. x_α is

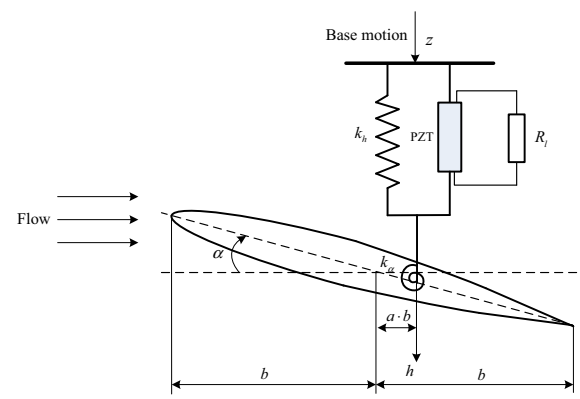

Fig. 1 Energy harvester under concurrent base and flow excitations

the dimensionless distance between the center of mass and the elastic axis. z represents the base excitation in the plunging direction. The terms m_T and m_W are the mass parameters of the airfoil. I_α is the mass moment of inertia about the elastic axis. L and T are the aerodynamic lift and moment acting on the airfoil. k_h and k_α are the stiffness in the plunging and pitching direction. R_l is the load resistance, and V is the voltage across the load resistance. C_p is the capacitance of the piezoelectric material. θ is the electromechanical coupling term of the piezoelectric material. c_h and c_α are the damping coefficients in the plunging and pitching direction.

A quasi-steady aerodynamic model with stall effects [24] is implemented for the computation of the aerodynamic loads

$$\begin{aligned} L &= \rho_\infty U_\infty^2 b c_{l\alpha}\left(\alpha_{eff} - c_s\alpha_{eff}^3\right) \\ T &= \rho_\infty U_\infty^2 b^2 c_{t\alpha}\left(\alpha_{eff} - c_s\alpha_{eff}^3\right) \end{aligned} \tag{2}$$

where α_{eff} is the effective angle of attack, U_∞ is the freestream velocity, $c_{l\alpha}$ and $c_{t\alpha}$ are the aerodynamic lift and moment coefficients. c_s is a nonlinear parameter associated with stall effects. The effective angle of attack α_{eff} is defined as follows

$$\alpha_{eff} = \alpha + \frac{\dot{h}}{U_\infty} + \left(\frac{1}{2} - a\right)\frac{b\dot{\alpha}}{U_\infty} \tag{3}$$

Now, the governing equations of the energy harvesting system can be rewritten as

$$\begin{aligned} &\mathbf{M}\ddot{\boldsymbol{\eta}} + \mathbf{K}\boldsymbol{\eta} + (\mathbf{C}\dot{\boldsymbol{\eta}} - \mathbf{C}_1\dot{z}) = \mathbf{Q}\left(\eta_2 + \frac{\dot{\eta}_1}{U_\infty} + b_0\dot{\eta}_2\right)^3 + \mathbf{P}V \\ &\dot{V} + R_0 V + \chi_p(\dot{\eta}_1 - \dot{z}) = 0 \end{aligned} \tag{4}$$

where

$$\begin{aligned} &\mathbf{M} = \begin{bmatrix} m_T & s_\alpha \\ s_\alpha & I_\alpha \end{bmatrix}, \quad \mathbf{K} = \begin{bmatrix} k_h & -L_s \\ 0 & k_\alpha - T_s \end{bmatrix}, \\ &\mathbf{C} = \begin{bmatrix} c_h - L_s/U_\infty & -L_s b_0 \\ -T_s/U_\infty & c_\alpha - T_s b_0 \end{bmatrix} \\ &\mathbf{C}_1 = \begin{pmatrix} c_h \\ 0 \end{pmatrix}, \quad \mathbf{Q} = \begin{pmatrix} L_s c_s \\ T_s c_s \end{pmatrix}, \quad \mathbf{P} = \begin{pmatrix} \theta \\ 0 \end{pmatrix}, \\ &\boldsymbol{\eta} = \begin{pmatrix} h \\ \alpha \end{pmatrix} = \begin{pmatrix} \eta_1 \\ \eta_2 \end{pmatrix} \\ &s_\alpha = m_W x_\alpha b, \quad L_s = -\rho_\infty U_\infty^2 b c_{l\alpha}, \end{aligned} \tag{5}$$

$$\begin{aligned} &T_s = \rho_\infty U_\infty^2 b^2 c_{t\alpha}, \quad c_{t\alpha} = \left(\frac{1}{2} + a\right) c_{l\alpha} \\ &b_0 = \left(\frac{1}{2} - a\right)\frac{b}{U_\infty}, \quad R_0 = \frac{1}{C_p R_l}, \quad \chi_p = \frac{\theta}{C_p} \end{aligned}$$

3 Approximate analytic solutions of internal resonance

In this section, the nonlinear dynamics of the energy harvester described by Eq. (4) are investigated via the method of multiple scales. Assume that the base excitation is harmonic, i.e., $z = z_0 \sin \Omega t$ where z_0 and Ω are the amplitude and frequency of base excitation.

It is assumed that the damping, electromechanical coupling and base excitation are small, and a small bookkeeping parameter ε is introduced to rescale the following variables:

$$\mathbf{C} \to \varepsilon^2\mathbf{C}, \mathbf{C}_1 \to \varepsilon^2\mathbf{C}_1, \mathbf{P} \to \varepsilon^2\mathbf{P}, \; z \to \varepsilon z \tag{6}$$

The governing equations of the energy harvesting system can be rewritten as

$$\begin{aligned} &\mathbf{M}\ddot{\boldsymbol{\eta}} + \mathbf{K}\boldsymbol{\eta} + \varepsilon^2\mathbf{C}\dot{\boldsymbol{\eta}} = \mathbf{Q}\left(\eta_2 + \frac{\dot{\eta}_1}{U_\infty} + b_0\dot{\eta}_2\right)^3 + \varepsilon^2\mathbf{P}V + \varepsilon^3\mathbf{C}_1\dot{z} \\ &\dot{V} + R_0 V + \chi_p\dot{\eta}_1 - \varepsilon\chi_p\dot{z} = 0 \end{aligned} \tag{7}$$

Since the nonlinearity of the energy harvesting system is cubic, the approximate analytic solution of Eq. (7) can be expressed as

$$\begin{aligned} \boldsymbol{\eta} &= \varepsilon\boldsymbol{\eta}_1(T_0, T_2, \cdots) + \varepsilon^3\boldsymbol{\eta}_3(T_0, T_2, \cdots) + O(\varepsilon^4) \\ V &= \varepsilon V_1(T_0, T_2, \cdots) + \varepsilon^3 V_3(T_0, T_2, \cdots) + O(\varepsilon^4) \end{aligned} \tag{8}$$

where $T_r = \varepsilon^r t$, $r = 0, \; 2, \; \cdots$ represent different time scales.

By substituting Eq. (8) into Eq. (7) and equating the same power of ε, one has

$$\begin{aligned} &\mathbf{M}D_0^2\boldsymbol{\eta}_1 + \mathbf{K}\boldsymbol{\eta}_1 = 0 \\ &D_0 V_1 + R_0 V_1 + \chi_p D_0\eta_{10} - \chi_p\dot{z} = 0 \\ &\mathbf{M}D_0^2\boldsymbol{\eta}_3 + \mathbf{K}\boldsymbol{\eta}_3 = -2\mathbf{M}D_2 D_0\boldsymbol{\eta}_1 - \mathbf{C}D_0\boldsymbol{\eta}_1 \\ &\quad + \mathbf{Q}\left(\eta_{21} + \frac{\dot{\eta}_{11}}{U_\infty} + b_0\dot{\eta}_{21}\right)^3 + \mathbf{P}V_1 + \mathbf{C}_1\dot{z} \\ &D_0 V_3 + R_0 V_3 = -D_2 V_1 - \chi_p\left(D_2\eta_{11} + D_0\eta_{31}\right) \end{aligned} \tag{9}$$

(10)

where $D_r = \partial/\partial T_r$ represent the partial differential operators. The first-order approximation solution can be obtained by solving Eq. (9) as follows

$$\begin{aligned}\boldsymbol{\eta}_1 &= A_1 e^{\mathrm{i}\omega_1 T_0}\mathbf{p}_1 + A_2 e^{\mathrm{i}\omega_2 T_0}\mathbf{p}_2 + cc \\ V_1 &= -\frac{\chi_p \mathrm{i}\omega_1}{\mathrm{i}\omega_1 + R_0} A_1 e^{\mathrm{i}\omega_1 T_0}\mathbf{p}_{11} - \frac{\chi_p \mathrm{i}\omega_2}{\mathrm{i}\omega_2 + R_0} \\ &\quad A_2 e^{\mathrm{i}\omega_2 T_0}\mathbf{p}_{21} + \frac{\chi_p \Omega}{\mathrm{i}\Omega + R_0} z_1 + cc\end{aligned} \tag{11}$$

where $z_1 = \frac{z_0}{2} e^{\mathrm{i}\Omega T_0}$ and cc represents the complex conjugate of the preceding terms. $\mathbf{p}_{11}$, $\mathbf{p}_{21}$ are the first entries of vectors $\mathbf{p}_1$, $\mathbf{p}_2$, respectively. ω_1, ω_2, $\mathbf{p}_1$, and $\mathbf{p}_2$ represent the natural frequencies and mode shapes of linearized energy harvesting system, respectively, satisfying the following eigenvalue problem

$$\omega_j^2 \mathbf{p}_j = \mathbf{M}^{-1}\mathbf{K}\mathbf{p}_j, \ (j = 1, 2) \tag{12}$$

ω_j and $\mathbf{p}_j$ can be obtained by solving Eq. (12) as follows

$$\begin{aligned}\omega_{1,2}^2 &= \frac{\Gamma_\omega \mp \sqrt{\Gamma_\omega^2 - 4\left(m_T I_\alpha - s_\alpha^2\right) k_h \left(k_\alpha - T_s\right)}}{2\left(m_T I_\alpha - s_\alpha^2\right)} \\ \mathbf{p}_j &= \begin{pmatrix}\mathbf{p}_{j1} \\ \mathbf{p}_{j2}\end{pmatrix} = \begin{pmatrix}\Lambda_j \\ 1\end{pmatrix}\end{aligned} \tag{13}$$

where

$$\begin{aligned}\Gamma_\omega &= m_T k_\alpha - m_T T_s + k_h I_\alpha + L_s s_\alpha \\ \Lambda_j &= \frac{L_s + \omega_j^2 s_\alpha}{k_h - \omega_j^2 m_T} = \frac{k_\alpha - T_s - \omega_j^2 I_\alpha}{\omega_j^2 s_\alpha}\end{aligned} \tag{14}$$

As the nonlinearity of the energy harvesting system is cubic, the system may undergo 3:1 internal resonance when the two natural frequencies satisfy the relationship $\omega_2 = 3\omega_1$. According to Eq. (13), the condition of 3:1 internal resonance can be obtained as follows

$$\begin{aligned}&\left(m_T k_\alpha - m_T T_s + k_h I_\alpha + L_s s_\alpha\right)^2 \\ &= \frac{100}{9}\left(m_T I_\alpha - s_\alpha^2\right) k_h \left(k_\alpha - T_s\right)\end{aligned} \tag{15}$$

Subsequently, the 3:1 internal resonance is investigated in detail when the base excitation frequency is close to the first modal frequency of the energy harvesting system. Two detuning parameters σ and σ_0 are defined as

$$\omega_2 = 3\omega_1 + \varepsilon^2\sigma, \quad \Omega = \omega_1 + \varepsilon^2\sigma_0 \tag{16}$$

which are used to describe the closeness of ω_2 to $3\omega_1$, and ω_1 to Ω, respectively.

By substituting Eq. (11) into Eq. (10) and eliminating the secular terms, the following solvability conditions can be obtained

$$\begin{aligned}&\mathbf{z}_1^{\mathrm{T}}[-2\mathbf{M}\mathrm{i}\omega_1\mathbf{p}_1 D_2 A_1 - \mathbf{C}\mathrm{i}\omega_1\mathbf{p}_1 A_1 \\ &+ \mathbf{P}\left(-\frac{\chi_p \mathrm{i}\omega_1}{\mathrm{i}\omega_1 + R_0} A_1 \mathbf{p}_{11}\right) \\ &+ \mathbf{Q}(a_{11} A_1^2 \bar{A}_1 + a_{12} A_1 A_2 \bar{A}_2) + \mathbf{Q} a_{13} A_2 \bar{A}_1^2 e^{\mathrm{i}\sigma T_2} \\ &+ \frac{1}{2}(\mathbf{F} + \mathbf{P}\frac{\chi_p \Omega z_0}{\mathrm{i}\Omega + R_0}) e^{\mathrm{i}\sigma_0 T_2}] = 0\end{aligned} \tag{17}$$

$$\begin{aligned}&\mathbf{z}_2^{\mathrm{T}}[-2\mathbf{M}\mathrm{i}\omega_2\mathbf{p}_2 D_2 A_2 - C\mathrm{i}\omega_2\mathbf{p}_2 A_2 \\ &+ \mathbf{P}\left(-\frac{\chi_p \mathrm{i}\omega_2}{\mathrm{i}\omega_2 + R_0} A_2 \mathbf{p}_{21}\right) \\ &+ \mathbf{Q}(a_{21} A_1 \bar{A}_1 A_2 + a_{22} A_2^2 \bar{A}_2) \\ &+ \mathbf{Q} a_{31} A_1^3 e^{-\mathrm{i}\sigma T_2}] = 0\end{aligned} \tag{18}$$

where $\mathbf{F} = \mathbf{C}_1 \Omega z_0$ and the details of a_{11}, a_{12}, a_{13}, a_{21}, a_{22}, a_{31} are presented in Appendix A. $\mathbf{z}_1$ and $\mathbf{z}_2$ are the solutions of the following equation

$$\omega_j^2 \mathbf{M}^{\mathrm{T}}\mathbf{z}_j = \mathbf{K}^{\mathrm{T}}\mathbf{z}_j, \ (j = 1, 2) \tag{19}$$

It needs to be noted that $\mathbf{z}_1$ and $\mathbf{z}_2$ are eigenvectors which can be normalized such that $\mathbf{z}_1^{\mathrm{T}}(2\mathbf{M}\omega_1\mathbf{p}_1) = 1$ and $\mathbf{z}_2^{\mathrm{T}}(2\mathbf{M}\omega_2\mathbf{p}_2) = 1$. By solving Eq. (19), $\mathbf{z}_1$ and $\mathbf{z}_2$ can be obtained as follows

$$\begin{aligned}\mathbf{z}_1 &= \frac{1}{N_{10}}\begin{pmatrix}\frac{\omega_1^2 s_\alpha}{k_h - \omega_1^2 m_T} \\ 1\end{pmatrix} = \frac{1}{N_{10}}\begin{pmatrix}\Lambda_1' \\ 1\end{pmatrix}, \\ \mathbf{z}_2 &= \frac{1}{N_{20}}\begin{pmatrix}\frac{\omega_2^2 s_\alpha}{k_h - \omega_2^2 m_T} \\ 1\end{pmatrix} = \frac{1}{N_{20}}\begin{pmatrix}\Lambda_2' \\ 1\end{pmatrix}\end{aligned} \tag{20}$$

where

$$\begin{aligned}N_{j0} = 2\omega_j &\left(\frac{\omega_j^2 s_\alpha m_T \left(L_s + \omega_j^2 s_\alpha\right)}{\left(k_h - \omega_j^2 m_T\right)^2} + \frac{s_\alpha^2 \omega_j^2}{k_h - \omega_j^2 m_T}\right. \\ &\left. + \frac{s_\alpha\left(L_s + \omega_j^2 s_\alpha\right)}{k_h - \omega_j^2 m_T} + I_\alpha\right), \ j = 1, 2\end{aligned} \tag{21}$$

By letting $A_1(T_2) = \frac{1}{2}a_1(T_2)\,e^{\mathrm{i}\beta_1(T_2)}$ and $A_2(T_2) = \frac{1}{2}a_2(T_2)\,e^{\mathrm{i}\beta_2(T_2)}$ in Eqs. (17) and (18), and separating the real and imaginary parts, the modulation equations are obtained as follows

$$\begin{aligned} &a_1' + \alpha_2 a_1 + \frac{1}{4}\alpha_4 a_1^3 + \frac{1}{4}\alpha_6 a_1 a_2^2 \\ &\quad + \frac{1}{4}a_1^2 a_2\left(\alpha_8\cos\gamma - \alpha_9\sin\gamma\right) \\ &\quad + \alpha_{10}\cos\gamma_0 - \alpha_{11}\sin\gamma_0 = 0 \end{aligned} \tag{22}$$

$$\begin{aligned} &a_1\beta_1' + \alpha_3 a_1 + \frac{1}{4}\alpha_5 a_1^3 + \frac{1}{4}\alpha_7 a_1 a_2^2 \\ &\quad + \frac{1}{4}a_1^2 a_2\left(\alpha_8\sin\gamma + \alpha_9\cos\gamma\right) \\ &\quad + \alpha_{11}\cos\gamma_0 + \alpha_{10}\sin\gamma_0 = 0 \end{aligned} \tag{23}$$

$$\begin{aligned} &a_2' + \gamma_2 a_2 + \frac{1}{4}\gamma_4 a_2^3 + \frac{1}{4}\gamma_6 a_1^2 a_2 \\ &\quad + \frac{1}{4}a_1^3\left(\gamma_8\cos\gamma + \gamma_9\sin\gamma\right) = 0 \end{aligned} \tag{24}$$

$$\begin{aligned} &a_2\beta_2' + \gamma_3 a_2 + \frac{1}{4}\gamma_5 a_2^3 + \frac{1}{4}\gamma_7 a_1^2 a_2 \\ &\quad + \frac{1}{4}a_1^3\left(\gamma_9\cos\gamma - \gamma_8\sin\gamma\right) = 0 \end{aligned} \tag{25}$$

where $(')$ denotes the derivative with respect to T_2 and the details of α_i and γ_i are listed in Appendix B. γ_0 and γ are defined as follows

$$\gamma_0(T_2) = \sigma_0 T_2 - \beta_1(T_2) \tag{26}$$

$$\gamma(T_2) = \beta_2(T_2) - 3\beta_1(T_2) + \sigma T_2 \tag{27}$$

Thus, the first-order approximate solution of 3:1 internal resonance can be analytically obtained as

$$\begin{aligned} \boldsymbol{\eta}_1 &= \varepsilon\left(a_1\mathbf{p}_1\cos\left(\omega_1 t + \beta_1\right) + a_2\mathbf{p}_2\cos\left(\omega_2 t + \beta_2\right)\right) \\ V_1 &= \varepsilon\left(-\frac{\chi_p\omega_1^2}{\omega_1^2 + R_0^2}a_1\Lambda_1\cos\left(\omega_1 t + \beta_1\right)\right. \\ &\quad \left. + \frac{\chi_p\omega_1 R_0}{\omega_1^2 + R_0^2}a_1\Lambda_1\sin\left(\omega_1 t + \beta_1\right)\right) \\ &\quad + \varepsilon\left(-\frac{\chi_p\omega_2^2}{\omega_2^2 + R_0^2}a_2\Lambda_2\cos\left(\omega_2 t + \beta_2\right)\right. \\ &\quad \left. + \frac{\chi_p\omega_2 R_0}{\omega_2^2 + R_0^2}a_2\Lambda_2\sin\left(\omega_2 t + \beta_2\right)\right) \\ &\quad + \varepsilon\frac{z_0\chi_p\Omega}{\Omega^2 + R_0^2}\left(R_0\cos\Omega t + \Omega\sin\Omega t\right) \end{aligned} \tag{28}$$

By combining Eqs. (23), (25), (26) and (27), one obtains the following equations

$$\begin{aligned} a_1\gamma_0' &= a_1\sigma_0 - a_1\beta_1' \\ &= a_1\sigma_0 + a_1\alpha_3 + \frac{1}{4}\alpha_5 a_1^3 + \frac{1}{4}\alpha_7 a_1 a_2^2 \\ &\quad + \frac{1}{4}a_1^2 a_2\left(\alpha_8\sin\gamma + \alpha_9\cos\gamma\right) \\ &\quad + \alpha_{10}\sin\gamma_0 + \alpha_{11}\cos\gamma_0 \end{aligned} \tag{29}$$

$$\begin{aligned} a_2\gamma' &= a_2\left(\beta_2' - 3\beta_1' + \sigma\right) \\ &= -\gamma_3 a_2 - \frac{1}{4}\gamma_5 a_2^3 - \frac{1}{4}\gamma_7 a_1^2 a_2 \\ &\quad - \frac{1}{4}a_1^3\left(\gamma_9\cos\gamma - \gamma_8\sin\gamma\right) + 3\alpha_3 a_2 \\ &\quad + \frac{3}{4}\alpha_5 a_1^2 a_2 + \frac{3}{4}\alpha_7 a_2^3 \\ &\quad + \frac{3}{4}a_1 a_2^2\left(\alpha_8\sin\gamma + \alpha_9\cos\gamma\right) + a_2\sigma \\ &\quad + 3\alpha_{10}\frac{a_2}{a_1}\sin\gamma_0 + 3\alpha_{11}\frac{a_2}{a_1}\cos\gamma_0 \end{aligned} \tag{30}$$

By letting $a_1' = 0$, $a_2' = 0$, $\gamma_0' = 0$ and $\gamma' = 0$, the steady-state response can be derived as follows:

$$\begin{aligned} &\alpha_2 a_1 + \frac{1}{4}\alpha_4 a_1^3 + \frac{1}{4}\alpha_6 a_1 a_2^2 \\ &\quad + \frac{1}{4}a_1^2 a_2\left(\alpha_8\cos\gamma - \alpha_9\sin\gamma\right) \\ &\quad + \alpha_{10}\cos\gamma_0 - \alpha_{11}\sin\gamma_0 = 0 \end{aligned} \tag{31}$$

$$\begin{aligned} &\gamma_2 a_2 + \frac{1}{4}\gamma_4 a_2^3 + \frac{1}{4}\gamma_6 a_1^2 a_2 \\ &\quad + \frac{1}{4}a_1^3\left(\gamma_8\cos\gamma + \gamma_9\sin\gamma\right) = 0 \end{aligned} \tag{32}$$

$$\begin{aligned} &a_1\sigma_0 + a_1\alpha_3 + \frac{1}{4}\alpha_5 a_1^3 + \frac{1}{4}\alpha_7 a_1 a_2^2 \\ &\quad + \frac{1}{4}a_1^2 a_2\left(\alpha_8\sin\gamma + \alpha_9\cos\gamma\right) \\ &\quad + \alpha_{10}\sin\gamma_0 + \alpha_{11}\cos\gamma_0 = 0 \end{aligned} \tag{33}$$

$$\begin{aligned} &\gamma_3 a_2 + \frac{1}{4}\gamma_5 a_2^3 + \frac{1}{4}\gamma_7 a_1^2 a_2 \\ &\quad + \frac{1}{4}a_1^3\left(\gamma_9\cos\gamma - \gamma_8\sin\gamma\right) - 3\alpha_3 a_2 - \frac{3}{4}\alpha_5 a_1^2 a_2 \\ &\quad - \frac{3}{4}\alpha_7 a_2^3 - \frac{3}{4}a_1 a_2^2\left(\alpha_8\sin\gamma + \alpha_9\cos\gamma\right) \\ &\quad - a_2\sigma - 3\alpha_{10}\frac{a_2}{a_1}\sin\gamma_0 - 3\alpha_{11}\frac{a_2}{a_1}\cos\gamma_0 = 0 \end{aligned} \tag{34}$$

Eqs. (31–34) reveal the relations of modal amplitudes a_1 and a_2 with respect to different system parameters. The amplitude of the harvested voltage can be derived based on Eqs. (28), (31–34).

It should be noted that the mode-coupled vibration of the energy harvesting system corresponds to the steady-state solutions of Eqs. (22), (24), (29) and (30). The stability of the mode-coupled vibration coincides with that of the corresponding constant solutions of the modulation equations. The vibration is asymptotically stable if the eigenvalues of the Jacobian matrix of the modulation equations at the corresponding steady-state solutions are in the left-half of complex plane.

4 Performance analysis of energy harvesting

In this section, the influence of several system parameters on the performance of the energy harvester is investigated based on analytic solutions. The parameters of the piezoaeroelastic energy harvester are listed in Table 1.

4.1 Characteristics of the output voltage

In order to demonstrate the influence of internal resonance on energy harvesting, a non-internal resonance case and a three-to-one internal resonance case are studied under concurrent base and flow excitations. The amplitude of the base excitation is set as $z_0 = 0.015$ m, and the frequency of the base excitation is close to the first modal frequency of the corresponding energy harvesting system.

For the three-to-one internal resonance case, the system parameters are listed in Table 1 and the air speed is set as 5 m/s according to the internal resonance condition shown by Eq. (15). The non-internal resonance case shows the nonlinear primary resonance response

Table 1 System parameters of the energy harvester

Physical properties			
b (m)	0.135	c_α(N m s)	0.001
x_α	0.331	θ (N/V)	0.00155
m_W (kg)	2.049	C_p (F)	1.2×10^{-7}
m_T (kg)	12.387	$R_l(\Omega)$	1.0×10^5
I_α(kg m^2)	0.0558	ρ_∞(kg/m^3)	1.225
k_h(N/m)	2380	$c_{l\alpha}$	6.28
k_α(N m/rad)	1.2	c_s	10.11
c_h(N s/m)	27.43	a(m)	-0.5

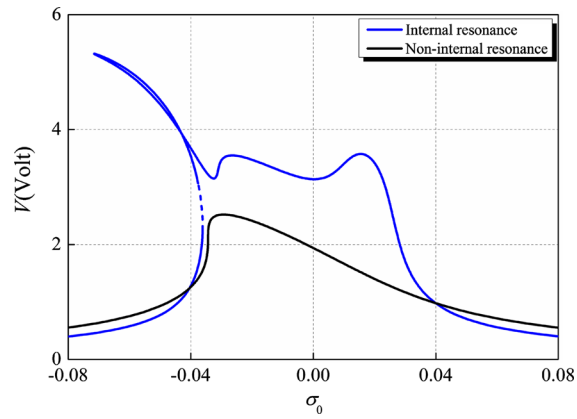

Fig. 2 Amplitude–frequency response of the harvested voltage

of the first mode away from the internal resonance, for which all the system parameters are the same as those of the internal resonance case except that $k_h = 2000$ N/m. For the non-internal resonance case and the three-to-one internal resonance case, the first modal frequencies are 4.691 rad/s and 4.681 rad/s, respectively. Figure 2 depicts a comparison of the amplitude–frequency response of the harvested voltage between the two cases. As shown in Fig. 2, the amplitude of the harvested voltage of the 3:1 internal resonance case is improved compared with that of the non-internal resonance case. Furthermore, an increase in the frequency bandwidth of the energy harvester is obtained with the internal resonance. This is due to the energy exchange between the two modes since the first mode is coupled with the second mode through the 3:1 internal resonance.

4.2 Influence of the base excitation

In this section, the influence of base excitation on energy harvesting is studied. At first, the effects of the amplitude of base excitation on the steady-state output voltage for the internal resonance case are investigated. The air speed is set as 2.22 m/s and the corresponding detuning parameter $\sigma = 0$ to rigorously meet the internal condition. Figure 3 illustrates the amplitude–frequency responses of the harvested voltage under different base excitations. As shown in Fig. 3, both the steady-state output voltage and the bandwidth increase with the amplitude of the base excitation. The amplitude–frequency response curves bend to the left indicating that the energy harvesting system of the

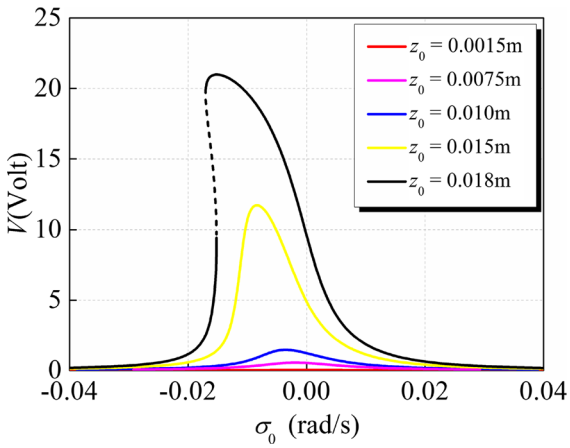

Fig. 3 Amplitude–frequency response of the harvested voltage for different excitation amplitudes

internal resonance case exhibits softening nonlinearity. Furthermore, with the increase in excitation amplitude, the solution becomes multivalued. There are three branches of solution: The solid lines represent stable solutions, and the dashed line represents the unstable saddles. In the multivalued region, at a given excitation frequency, the energy harvesting system may exhibit higher or lower amplitude responses depending on the initial condition and the frequency sweep direction.

Subsequently, the effects of the frequency of base excitation on the steady-state output voltage for the internal resonance case are investigated. Figures 4 and 5 illustrate the variation of the steady-state output voltage with the amplitude of the base excitation for different excitation frequencies. As shown in Fig. 4, the steady-state output voltage increases with the excitation amplitude. Furthermore, it decreases with the increase in the detuning parameter σ_0, since the excitation frequency moves away from the frequency of the first mode. As shown in Fig. 5, the output voltage amplitude is strongly dependent on the sign of σ_0. Larger output voltage amplitude can be obtained for the lower excitation frequency which is consistent with the aforementioned system's softening-type nonlinearity.

4.3 Influence of the air speed

The air speed $U_\infty = 2.22$ m/s, for which the detuning parameter $\sigma = 0$, results in three-to-one internal resonance. If the air speed changes around the threshold value 2.22 m/s, the 3:1 internal resonance phenomenon still exists. This section studies the effects of air speed on energy harvesting.

Figure 6 depicts the amplitude–frequency response curves for different excitation amplitudes when the air speed is 5 m/s and the corresponding detuning parameter $\sigma = -0.228$ rad/s. The results show that both the output voltage and the bandwidth of the energy harvester increase as the excitation amplitude increases. Furthermore, there are two peaks in the amplitude–frequency response curves when the excitation amplitude is larger than a threshold, which is different from the results shown in Fig. 3. The first peak, which is large and bends to the left, occurs to the left of $\sigma_0 = 0$. The second peak, which is small and has no bending, occurs to the right of $\sigma_0 = 0$. A wider frequency bandwidth of the energy harvesting is obtained due to the existence of the two peaks. In addition, the amplitude–frequency response curves bend more to the left which indicates the system's softening-type nonlinearity.

Figure 7 illustrates the amplitude–frequency response curves of the harvested voltage with base excitation amplitude $z_0 = 0.015$ m for different air speeds. As shown in Fig. 7, there is one peak in the amplitude–frequency response curve for small air speed, while the curves have two peaks for large air speed. The results indicate that the relatively large air speed can broaden the bandwidth of the energy harvester if the condition of three-to-one internal resonance $\omega_2 \approx 3\omega_1$ can be fulfilled. Hence, larger air speed at which the internal resonance condition is satisfied is preferred in order to broaden the frequency bandwidth of the energy harvesting system.

4.4 Influence of the electric load

The effects of electric load, another important parameter of the energy harvesting system, are investigated here.

Figures 8 and 9 illustrate the variations of output voltage and the harvested power with the electric load, under base excitations with the amplitude $z_0 = 0.015$ m and different frequencies. The harvested power is determined as $P = V_{\mathrm{RMS}}^2/R_l$ where V_{RMS} is the Root-Mean-Square (RMS) value of the output voltage. As shown in Fig. 8, the output voltage increases rapidly with electric load in the relatively small load range (below 250 KΩ) and then increases slowly, or even decreases when the electric load is large. Figure 9

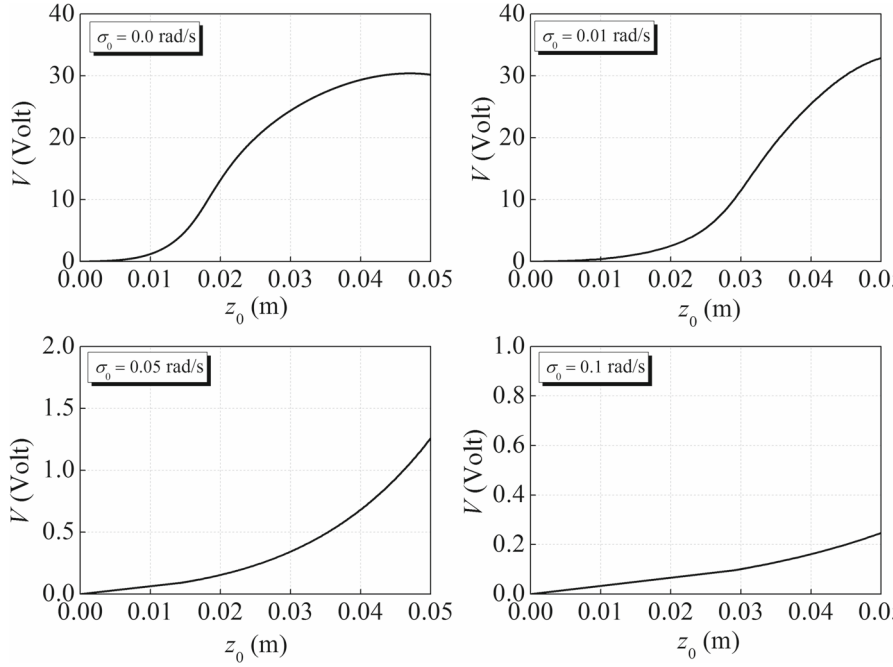

Fig. 4 Variation of the steady-state output voltage amplitude with the excitation amplitude for different excitation frequencies

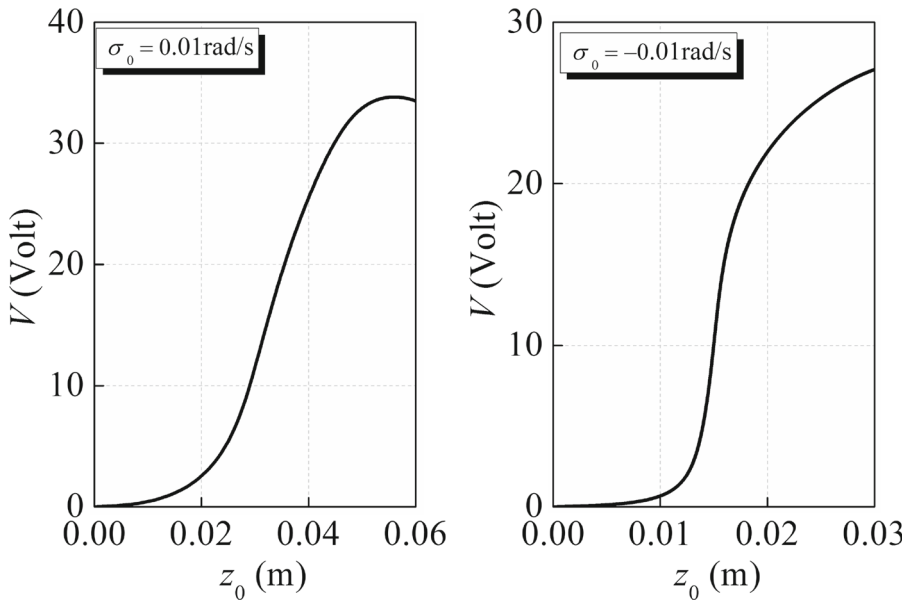

Fig. 5 Variation of the steady-state output voltage amplitude with the excitation amplitude for $|\sigma_0| = 0.01$ rad/s

shows that there exists an optimal electric load to generate the highest power. The output power increases rapidly with the electric load in the relatively small load range (below the optimal load) and then decreases when the load continues to increase away from the optimal load. The results demonstrate that electric load plays an important role in energy harvesting, and an optimal electric load can be determined easily by analytic analysis. Furthermore, the results indicate that the amplitudes of output voltage and power decrease with the increase in $|\sigma_0|$. When $|\sigma_0|$ is small, the base excitation with low frequency ($\sigma_0 < 0$) will yield larger output voltage and power.

Figure 10 demonstrates the variations of output voltage and power with the electric load for the energy harvesters with and without internal resonance. As

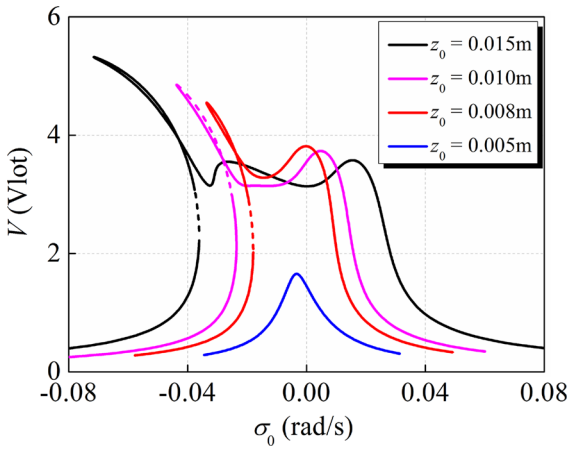

Fig. 6 Variation of the steady-state output voltage amplitude with the excitation frequency for different excitation amplitudes with $U_\infty = 5$ m/s

shown in Fig. 10, both the output voltage and the power increase rapidly with the electric load in the relatively small load range. They will decrease with the increasing electric load when it is larger than the optimal load. Besides, the optimal loads for the energy harvesters with and without internal resonance are nearly the same. The numerical results show that both the output voltage and the power of the internal resonance case are apparently improved due to the existence of three-to-one internal resonance.

5 Numerical validations

In this section, the numerical solutions of the energy harvester system Eq. (1) are compared with the approximate analytic solutions given by Eq. (28) in order to validate the analytic method.

Figure 11 illustrates a comparison between the approximate analytic solutions and the numerical solutions. In these cases, the physical parameters are set as shown in Table 1 and $U_\infty = 2.22$ m/s. The initial condition is set as follows: $\left[a_{10}\ a_{20}\ \beta_{10}\ \beta_{20}\right]^{\mathrm{T}} = \left[0.001\ 0.0155\ 0\ 0\right]^{\mathrm{T}}$. As shown in Fig. 11, a good agreement between the numerical solutions and the approximate analytic solutions is achieved. In addition, in order to validate the multi-scale analysis, the approximate analytic solutions are compared with the numerical solutions for different perturbation parameters. The time histories of the pitch angle and voltage are presented in Figs. 12, 13, 14 and 15. For small perturbation parameters $\varepsilon = 0.01$ and $\varepsilon = 0.1$, the approximate analytic results are in good agreement with the numerical results as shown in Figs. 12 and 13, respectively. For large perturbation parameter $\varepsilon = 0.5$, the

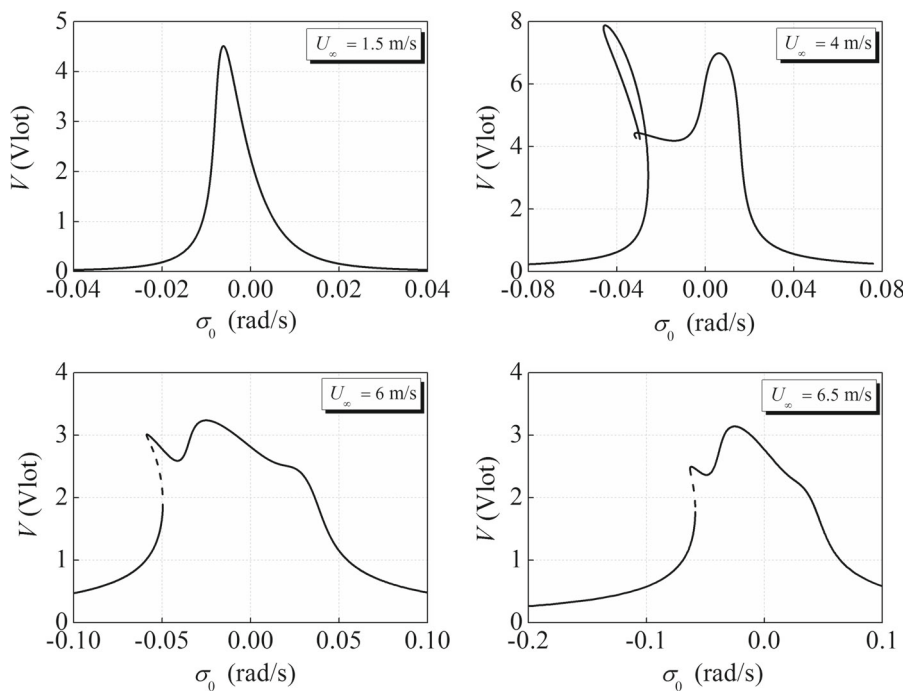

Fig. 7 Variation of the steady-state output voltage amplitude with the excitation frequency for different air speeds

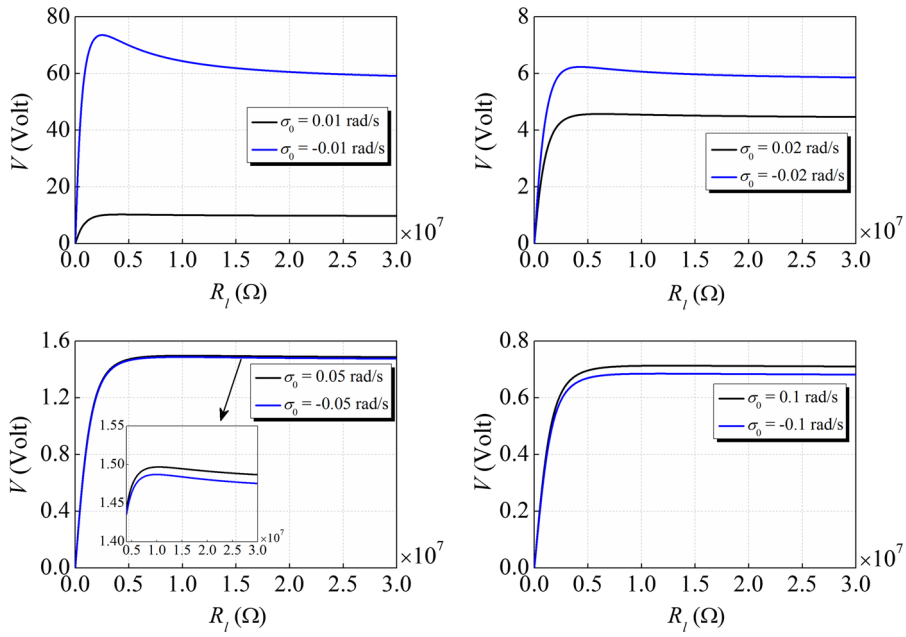

Fig. 8 Variation of the steady-state output voltage with the electric load

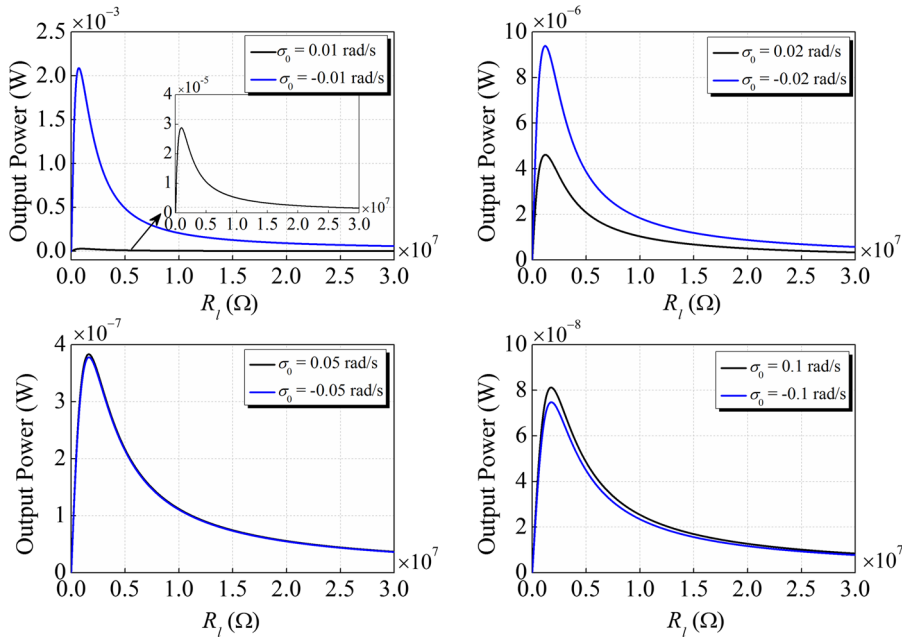

Fig. 9 Variation of the output power with the electric load

approximate analytic results are still in good agreement with the numerical results as shown in Fig. 14. For very large perturbation parameter $\varepsilon = 1.0$, there are apparent differences between the approximate analytic results and the numerical results as shown in Fig. 15, especially when time is greater than 12 s. These numerical results demonstrate that the analytic analyses are valid for small perturbation parameters.

6 Conclusions

This study investigates internal resonance to further explore the potential of energy harvesting under concurrent base and flow excitations. The approximate analytic solutions of the energy harvesting with internal resonance are obtained via the method of multiple scales. The effects of system parameters on the har-

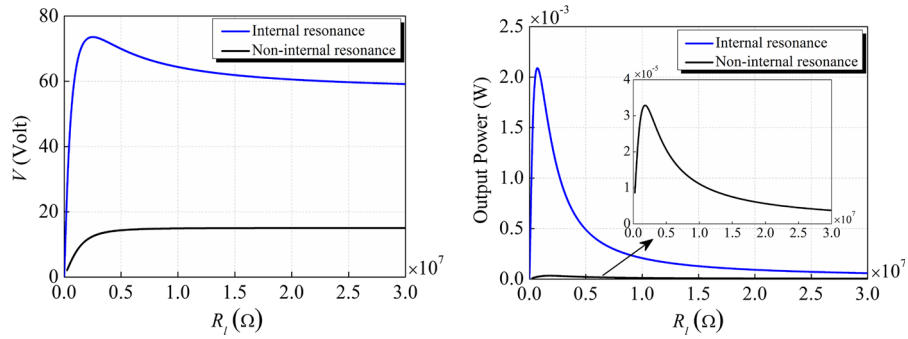

Fig. 10 Variation of the steady-state output voltage and power with the electric load for internal resonance and non-internal resonance cases

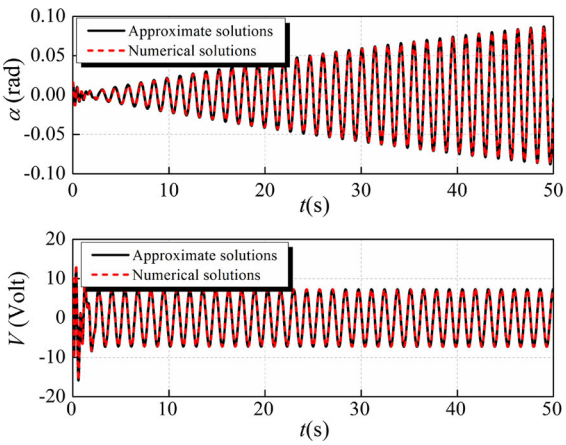

Fig. 11 Comparison between the approximate solutions and the numerical solutions

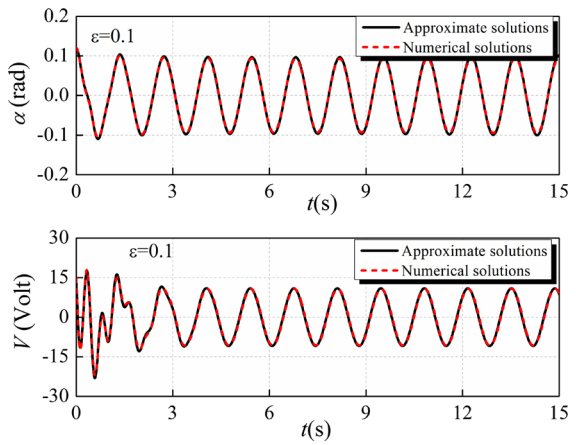

Fig. 13 Comparison between the approximate solutions and the numerical solutions for $\varepsilon = 0.1$

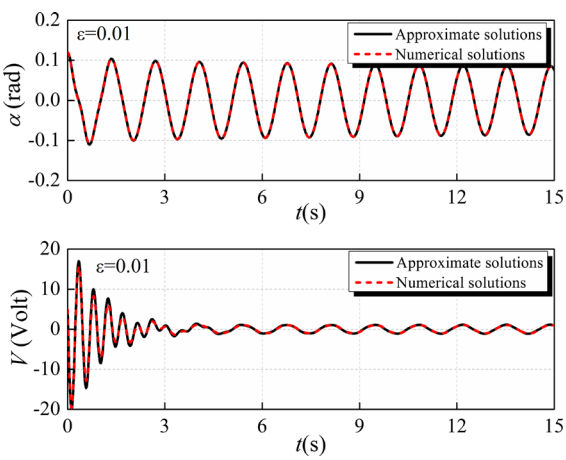

Fig. 12 Comparison between the approximate solutions and the numerical solutions for $\varepsilon = 0.01$

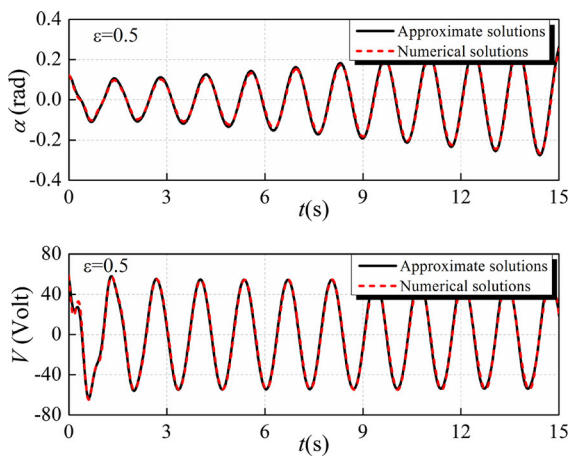

Fig. 14 Comparison between the approximate solutions and the numerical solutions for $\varepsilon = 0.5$

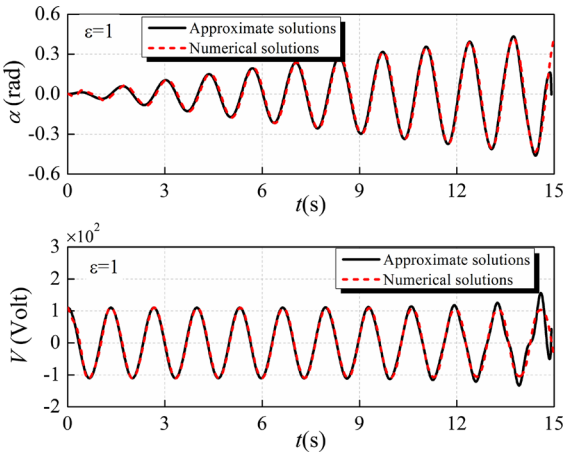

Fig. 15 Comparison between the approximate solutions and the numerical solutions for $\varepsilon = 1$

vester performance can be analyzed analytically, and the following conclusions are drawn:

The superiority of the internal resonance design is demonstrated compared to the case without internal resonance. Both the steady-state output voltage amplitude and the bandwidth of the energy harvester increase with base excitation amplitude. The energy harvesting system exhibits softening-type nonlinearity. There exists an optimal electric load to generate the highest power. The approximate analytic solutions are in good agreement with numerical solutions. Furthermore, the approximate analytic solutions and their bifurcation analysis obtained in this study can provide an essential reference for both numerical and experimental studies of such a kind of energy harvester.

Acknowledgements This work was supported by the Starting Research Foundation of Nanjing Tech University under grant 3827400225.

Compliance with Ethical Standards

Conflicts of interest The authors declare that there is no conflict of interest in relation to this article.

Appendix A

The details of a_{ij} in Eqs. (17) and (18) read

$$
\begin{aligned}
a_{11} &= 3\mathbf{p}_{12}^3 + 6U_\infty\omega_1^2 b_0\mathbf{p}_{11}\mathbf{p}_{12}^2 + 3b_0^2\omega_1^2\mathbf{p}_{12}^3 \\
&\quad + 3U_\infty^2\omega_1^2\mathbf{p}_{11}^2\mathbf{p}_{12} + \mathrm{i}(3\mathbf{p}_{12}^2 U_\infty\omega_1\mathbf{p}_{11} + 3b_0^3\omega_1^3\mathbf{p}_{12}^3 \\
&\quad + 3U_\infty^3\omega_1^3\mathbf{p}_{11}^3 + 9U_\infty b_0^2\omega_1^3\mathbf{p}_{11}\mathbf{p}_{12}^2 \\
&\quad + 9U_\infty^2\omega_1^3 b_0\mathbf{p}_{11}^2\mathbf{p}_{12} + 3b_0\omega_1\mathbf{p}_{12}^3) \\
&= a_{110} + \mathrm{i}a_{111} \\
a_{12} &= 6\mathbf{p}_{12}\mathbf{p}_{22}^2 + 12U_\infty b_0\omega_2^2\mathbf{p}_{12}\mathbf{p}_{21}\mathbf{p}_{22} \\
&\quad + 6U_\infty^2\omega_2^2\mathbf{p}_{12}\mathbf{p}_{21}^2 + 6b_0^2\omega_2^2\mathbf{p}_{12}\mathbf{p}_{22}^2 \\
&\quad + \mathrm{i}(6U_\infty\omega_1\mathbf{p}_{11}\mathbf{p}_{22}^2 + 12U_\infty^2\omega_1\omega_2^2 b_0\mathbf{p}_{11}\mathbf{p}_{21}\mathbf{p}_{22} \\
&\quad + 12U_\infty b_0^2\omega_1\omega_2^2\mathbf{p}_{12}\mathbf{p}_{21}\mathbf{p}_{22} \\
&\quad + 6U_\infty b_0^2\omega_1\omega_2^2\mathbf{p}_{11}\mathbf{p}_{22}^2 \\
&\quad + 6U_\infty^3\omega_1\omega_2^2\mathbf{p}_{11}\mathbf{p}_{21}^2 + 6b_0\omega_1\mathbf{p}_{12}\mathbf{p}_{22}^2 \\
&\quad + 6b_0^3\omega_1\omega_2^2\mathbf{p}_{12}\mathbf{p}_{22}^2 \\
&\quad + 6U_\infty^2 b_0\omega_1\omega_2^2\mathbf{p}_{12}\mathbf{p}_{21}^2) \\
&= a_{120} + \mathrm{i}a_{121} \\
a_{13} &= 6b_0^2\omega_1\omega_2\mathbf{p}_{12}^2\mathbf{p}_{22} + 6U_\infty^2\omega_1\omega_2\mathbf{p}_{11}\mathbf{p}_{12}\mathbf{p}_{21} \\
&\quad - 3U_\infty^2\omega_1^2\mathbf{p}_{11}^2\mathbf{p}_{22} - 6U_\infty\omega_1^2 b_0\mathbf{p}_{11}\mathbf{p}_{12}\mathbf{p}_{22} \\
&\quad - 3b_0^2\omega_1^2\mathbf{p}_{12}^2\mathbf{p}_{22} + 6U_\infty b_0\omega_1\omega_2\mathbf{p}_{11}\mathbf{p}_{12}\mathbf{p}_{22} \\
&\quad + 6U_\infty b_0\omega_1\omega_2\mathbf{p}_{12}^2\mathbf{p}_{21} + 3\mathbf{p}_{12}^2\mathbf{p}_{22} \\
&\quad + \mathrm{i}(-6U_\infty\omega_1\mathbf{p}_{11}\mathbf{p}_{12}\mathbf{p}_{22} + 3b_0\omega_2\mathbf{p}_{12}^2\mathbf{p}_{22} \\
&\quad - 6U_\infty^2 b_0\omega_1^2\omega_2\mathbf{p}_{11}\mathbf{p}_{12}\mathbf{p}_{21} + 3U_\infty\omega_2\mathbf{p}_{12}^2\mathbf{p}_{21} \\
&\quad - 6U_\infty\omega_1^2\omega_2 b_0^2\mathbf{p}_{11}\mathbf{p}_{12}\mathbf{p}_{22} - 6b_0\omega_1\mathbf{p}_{12}^2\mathbf{p}_{22} \\
&\quad - 3U_\infty^2 b_0\omega_1^2\omega_2\mathbf{p}_{11}^2\mathbf{p}_{22} - 3b_0^3\omega_1^2\omega_2\mathbf{p}_{12}^2\mathbf{p}_{22} \\
&\quad - 3U_\infty^3\omega_1^2\omega_2\mathbf{p}_{21}\mathbf{p}_{11}^2 - 3U_\infty b_0^2\omega_1^2\omega_2\mathbf{p}_{12}^2\mathbf{p}_{21}) \\
&= a_{130} + \mathrm{i}a_{131} \\
a_{21} &= 6b_0^2\omega_1^2\mathbf{p}_{12}^2\mathbf{p}_{22} + 12U_\infty b_0\omega_1^2\mathbf{p}_{11}\mathbf{p}_{12}\mathbf{p}_{22} \\
&\quad + 6U_\infty^2\omega_1^2\mathbf{p}_{11}^2\mathbf{p}_{22} + 6\mathbf{p}_{12}^2\mathbf{p}_{22} + \mathrm{i}(6b_0^3\omega_1^2\omega_2\mathbf{p}_{12}^2\mathbf{p}_{22} \\
&\quad + 12U_\infty\omega_1^2\omega_2 b_0^2\mathbf{p}_{11}\mathbf{p}_{12}\mathbf{p}_{22} + 6b_0\omega_2\mathbf{p}_{12}^2\mathbf{p}_{22} \\
&\quad + 6U_\infty b_0^2\omega_1^2\omega_2\mathbf{p}_{12}^2\mathbf{p}_{21} \ + 6U_\infty\omega_2\mathbf{p}_{12}^2\mathbf{p}_{21} \\
&\quad + 6U_\infty^3\omega_1^2\omega_2\mathbf{p}_{11}^2\mathbf{p}_{21} + 12U_\infty^2 b_0\omega_1^2\omega_2\mathbf{p}_{11}\mathbf{p}_{12}\mathbf{p}_{21} \\
&\quad + 6U_\infty^2 b_0\omega_1^2\omega_2\mathbf{p}_{11}^2\mathbf{p}_{22}) \\
&= a_{210} + \mathrm{i}a_{211} \\
a_{22} &= 3b_0^2\omega_2^2\mathbf{p}_{22}^3 + 3\mathbf{p}_{22}^3 + 3U_\infty^2\omega_2^2\mathbf{p}_{22}\mathbf{p}_{21}^2 \\
&\quad + 6U_\infty b_0\omega_2^2\mathbf{p}_{21}\mathbf{p}_{22}^2 + \mathrm{i}(3U_\infty^3\omega_2^3\mathbf{p}_{21}^3 + 3b_0\omega_2\mathbf{p}_{22}^3 \\
&\quad + 9U_\infty b_0^2\omega_2^3\mathbf{p}_{21}\mathbf{p}_{22}^2 + 3U_\infty\omega_2\mathbf{p}_{21}\mathbf{p}_{22}^2 \\
&\quad + 3b_0^3\omega_2^3\mathbf{p}_{22}^3 + 9U_\infty^2 b_0\omega_2^3\mathbf{p}_{22}\mathbf{p}_{21}^2) \\
&= a_{220} + \mathrm{i}a_{221} \\
a_{31} &= 3b_0^2\omega_1^2\mathbf{p}_{12}^3 + 6U_\infty b_0\omega_1^2\mathbf{p}_{12}^2\mathbf{p}_{11} + 3U_\infty^2\omega_1^2\mathbf{p}_{12}\mathbf{p}_{11}^2 \\
&\quad - \mathbf{p}_{12}^3 + \mathrm{i}(U_\infty^3\omega_1^3\mathbf{p}_{11}^3 - 3b_0\omega_1\mathbf{p}_{12}^3 \\
&\quad + 3U_\infty^2 b_0\omega_1^3\mathbf{p}_{11}^2\mathbf{p}_{12} - 3U_\infty\omega_1\mathbf{p}_{12}^2\mathbf{p}_{11} + b_0^3\omega_1^3\mathbf{p}_{12}^3 \\
&\quad + 3U_\infty\omega_1^3 b_0^2\mathbf{p}_{12}^2\mathbf{p}_{11}) \\
&= a_{310} + \mathrm{i}a_{311}
\end{aligned}
$$

Appendix B

The details of α_i and γ_i in Eqs. (22–25) read

$$\begin{aligned}
\alpha_2 &= \mathbf{z}_1^{\mathrm{T}}\left(\mathbf{C}\omega_1\mathbf{p}_1 + \mathbf{P}\frac{\chi_p\omega_1 R_0}{\omega_1^2+R_0^2}\mathbf{p}_{11}\right)\\
&= \frac{1}{N_{10}}\left(\Lambda_1'\left(\omega_1\Lambda_1\left(c_h - \frac{L_s}{U_\infty}\right) - \omega_1 L_s b_0\right.\right.\\
&\quad \left.+\theta\Lambda_1\frac{\chi_p\omega_1 R_0}{\omega_1^2+R_0^2}\right) - \frac{T_s}{U_\infty}\omega_1\Lambda_1 + \omega_1 c_\alpha\\
&\quad \left.-\omega_1 T_s b_0\right)\\
\alpha_3 &= -\mathbf{z}_1^{\mathrm{T}}\mathbf{P}\frac{\chi_p\omega_1^2}{\omega_1^2+R_0^2}\mathbf{p}_{11} = -\frac{1}{N_{10}}\Lambda_1'\theta\Lambda_1\\
&\quad \frac{\omega_1^2\chi_p}{\omega_1^2+R_0^2}\\
\alpha_4 &= -\mathbf{z}_1^{\mathrm{T}}\mathbf{Q}a_{111}\\
&= -\frac{1}{N_{10}}\left(-\Lambda_1' c_s L_s - c_s T_s\right)\left(3\mathbf{p}_{12}^2 U_\infty\omega_1\mathbf{p}_{11}\right.\\
&\quad +3b_0^3\omega_1^3\mathbf{p}_{12}^3 + 3U_\infty^3\omega_1^3\mathbf{p}_{11}^3 + 9U_\infty b_0^2\omega_1^3\mathbf{p}_{11}\mathbf{p}_{12}^2\\
&\quad \left.+9U_\infty^2\omega_1^3 b_0\mathbf{p}_{11}^2\mathbf{p}_{12} + 3b_0\omega_1\mathbf{p}_{12}^3\right)\\
\alpha_5 &= \mathbf{z}_1^{\mathrm{T}}\mathbf{Q}a_{110}\\
&= \frac{1}{N_{10}}\left(-\Lambda_1' c_s L_s - c_s T_s\right)\\
&\quad \left(3\mathbf{p}_{12}^3 + 6U_\infty\omega_1^2 b_0\mathbf{p}_{11}\mathbf{p}_{12}^2 + 3b_0^2\omega_1^2\mathbf{p}_{12}^3\right.\\
&\quad \left.+3U_\infty^2\omega_1^2\mathbf{p}_{11}^2\mathbf{p}_{12}\right)\\
\alpha_6 &= -\mathbf{z}_1^{\mathrm{T}}\mathbf{Q}a_{121}\\
&= -\frac{1}{N_{10}}\left(-\Lambda_1' c_s L_s - c_s T_s\right)\left(12U_\infty^2\omega_1\omega_2^2 b_0\right.\\
&\quad \mathbf{p}_{11}\mathbf{p}_{21}\mathbf{p}_{22} + 6b_0^3\omega_1\omega_2^2\mathbf{p}_{12}\mathbf{p}_{22}^2\\
&\quad + 12U_\infty b_0^2\omega_1\omega_2^2\mathbf{p}_{12}\mathbf{p}_{21}\mathbf{p}_{22} + 6U_\infty^3\omega_1\omega_2^2\mathbf{p}_{11}\mathbf{p}_{21}^2\\
&\quad +6U_\infty b_0^2\omega_1\omega_2^2\mathbf{p}_{11}\mathbf{p}_{22}^2\\
&\quad + 6U_\infty\omega_1\mathbf{p}_{11}\mathbf{p}_{22}^2 + 6U_\infty^2 b_0\omega_1\omega_2^2\mathbf{p}_{12}\mathbf{p}_{21}^2\\
&\quad \left.+6b_0\omega_1\mathbf{p}_{12}\mathbf{p}_{22}^2\right)\\
\alpha_7 &= \mathbf{z}_1^{\mathrm{T}}\mathbf{Q}a_{120}\\
&= \frac{1}{N_{10}}\left(-\Lambda_1' c_s L_s - c_s T_s\right)\\
&\quad \left(6\mathbf{p}_{12}\mathbf{p}_{22}^2 + 12U_\infty b_0\omega_2^2\mathbf{p}_{12}\mathbf{p}_{21}\mathbf{p}_{22}\right.\\
&\quad \left.+6U_\infty^2\omega_2^2\mathbf{p}_{12}\mathbf{p}_{21}^2 + 6b_0^2\omega_2^2\mathbf{p}_{12}\mathbf{p}_{22}^2\right)\\
\alpha_8 &= -\mathbf{z}_1^{\mathrm{T}}\mathbf{Q}a_{131}\\
&= -\frac{1}{N_{10}}\left(-\Lambda_1' c_s L_s - c_s T_s\right)\left(-6U_\infty\omega_1\mathbf{p}_{11}\mathbf{p}_{12}\mathbf{p}_{22}\right.\\
&\quad +3b_0\omega_2\mathbf{p}_{12}^2\mathbf{p}_{22} - 6U_\infty^2 b_0\omega_1^2\omega_2\mathbf{p}_{11}\mathbf{p}_{12}\mathbf{p}_{21}\\
&\quad -6U_\infty\omega_1^2\omega_2 b_0^2\mathbf{p}_{11}\mathbf{p}_{12}\mathbf{p}_{22} + 3U_\infty\omega_2\mathbf{p}_{12}^2\mathbf{p}_{21}\\
&\quad -3U_\infty^3\omega_1^2\omega_2\mathbf{p}_{21}\mathbf{p}_{11}^2 - 6b_0\omega_1\mathbf{p}_{12}^2\mathbf{p}_{22}\\
&\quad -3U_\infty b_0^2\omega_1^2\omega_2\mathbf{p}_{12}^2\mathbf{p}_{21} - 3U_\infty^2 b_0\omega_1^2\omega_2\mathbf{p}_{11}^2\mathbf{p}_{22}\\
&\quad \left.-3b_0^3\omega_1^2\omega_2\mathbf{p}_{12}^2\mathbf{p}_{22}\right)\\
\alpha_9 &= \mathbf{z}_1^{\mathrm{T}}\mathbf{Q}a_{130}\\
&= \frac{1}{N_{10}}\left(-\Lambda_1' c_s L_s - c_s T_s\right)\left(6b_0^2\omega_1\omega_2\mathbf{p}_{12}^2\mathbf{p}_{22}\right.\\
&\quad -3b_0^2\omega_1^2\mathbf{p}_{12}^2\mathbf{p}_{22} + 6U_\infty^2\omega_1\omega_2\mathbf{p}_{11}\mathbf{p}_{12}\mathbf{p}_{21} + 3\mathbf{p}_{12}^2\mathbf{p}_{22}\\
&\quad -6U_\infty\omega_1^2 b_0\mathbf{p}_{11}\mathbf{p}_{12}\mathbf{p}_{22} + 6U_\infty b_0\omega_1\omega_2\mathbf{p}_{11}\mathbf{p}_{12}\mathbf{p}_{22}\\
&\quad \left.+6U_\infty b_0\omega_1\omega_2\mathbf{p}_{12}^2\mathbf{p}_{21} - 3U_\infty^2\omega_1^2\mathbf{p}_{11}^2\mathbf{p}_{22}\right)\\
\alpha_{10} &= \mathbf{z}_1^{\mathrm{T}}\mathbf{P}\frac{\chi_p\Omega^2}{\Omega^2+R_0^2}z_0 = \frac{1}{N_{10}}\Lambda_1'\theta\frac{\chi_p\Omega^2}{\Omega^2+R_0^2}z_0\\
\alpha_{11} &= \mathbf{z}_1^{\mathrm{T}}\left(\mathbf{C}_1\Omega z_0 + \mathbf{P}\frac{\chi_p\Omega R_0}{\Omega^2+R_0^2}z_0\right)\\
&= \frac{1}{N_{10}}\Lambda_1'\left(c_h\Omega + \theta\frac{\chi_p\Omega R_0}{\Omega^2+R_0^2}\right)z_0\\
\gamma_2 &= \mathbf{z}_2^{\mathrm{T}}(\mathbf{C}\omega_2\mathbf{p}_2 + \mathbf{P}\frac{\chi_p\omega_2 R_0}{\omega_2^2+R_0^2}\mathbf{p}_{21})\\
&= \frac{1}{N_{20}}\left(\Lambda_2'\left(\omega_2\Lambda_2\left(c_h - \frac{L_s}{U_\infty}\right) - \omega_2 L_s b_0\right.\right.\\
&\quad \left.+\theta\Lambda_2\frac{\chi_p\omega_2 R_0}{\omega_2^2+R_0^2}\right) - \frac{T_s}{U_\infty}\omega_2\Lambda_2 + \omega_2 c_\alpha\\
&\quad \left.-\omega_2 T_s b_0\right)\\
\gamma_3 &= -\mathbf{z}_2^{\mathrm{T}}\mathbf{P}\frac{\chi_p\omega_2^2}{\omega_2^2+R_0^2}\mathbf{p}_{21} = -\frac{1}{N_{20}}\Lambda_2'\theta\Lambda_2\\
&\quad \frac{\omega_2^2\chi_p}{\omega_2^2+R_0^2}\\
\gamma_4 &= -\mathbf{z}_2^{\mathrm{T}}\mathbf{Q}a_{221}\\
&= -\frac{1}{N_{20}}\left(-\Lambda_2' c_s L_s - c_s T_s\right)\left(3U_\infty^3\omega_2^3\mathbf{p}_{21}^3\right.
\end{aligned}$$

$$+3b_0\omega_2\mathbf{p}_{22}^3+9U_\infty b_0^2\omega_2^3\mathbf{p}_{21}\mathbf{p}_{22}^2+3U_\infty\omega_2\mathbf{p}_{21}\mathbf{p}_{22}^2$$
$$+9U_\infty^2 b_0\omega_2^3\mathbf{p}_{22}\mathbf{p}_{21}^2+3b_0^3\omega_2^3\mathbf{p}_{22}^3)$$

$$\gamma_5=\mathbf{z}_2^{\mathrm{T}}\mathbf{Q}a_{220}$$
$$=\frac{1}{N_{20}}\left(-\Lambda_2' c_s L_s-c_s T_s\right)$$
$$(3b_0^2\omega_2^2\mathbf{p}_{22}^3+3\mathbf{p}_{22}^3+3U_\infty^2\omega_2^2\mathbf{p}_{22}\mathbf{p}_{21}^2$$
$$+6U_\infty b_0\omega_2^2\mathbf{p}_{21}\mathbf{p}_{22}^2)$$

$$\gamma_6=-\mathbf{z}_2^{\mathrm{T}}\mathbf{Q}a_{211}$$
$$=-\frac{1}{N_{20}}\left(-\Lambda_2' c_s L_s-c_s T_s\right)(12U_\infty\omega_1^2\omega_2 b_0^2$$
$$\mathbf{p}_{11}\mathbf{p}_{12}\mathbf{p}_{22}+6b_0^3\omega_1^2\omega_2\mathbf{p}_{12}^2\mathbf{p}_{22}+6b_0\omega_2\mathbf{p}_{12}^2\mathbf{p}_{22}$$
$$+6U_\infty^3\omega_1^2\omega_2\mathbf{p}_{11}^2\mathbf{p}_{21}+12U_\infty^2 b_0\omega_1^2\omega_2\mathbf{p}_{11}\mathbf{p}_{12}\mathbf{p}_{21}$$
$$+6U_\infty^2 b_0\omega_1^2\omega_2\mathbf{p}_{11}^2\mathbf{p}_{22}+6U_\infty\omega_2\mathbf{p}_{12}^2\mathbf{p}_{21}$$
$$+6U_\infty b_0^2\omega_1^2\omega_2\mathbf{p}_{12}^2\mathbf{p}_{21})$$

$$\gamma_7=\mathbf{z}_2^{\mathrm{T}}\mathbf{Q}a_{210}$$
$$=\frac{1}{N_{20}}\left(-\Lambda_2' c_s L_s-c_s T_s\right)\Big(6b_0^2\omega_1^2\mathbf{p}_{12}^2\mathbf{p}_{22}$$
$$+12U_\infty b_0\omega_1^2\mathbf{p}_{11}\mathbf{p}_{12}\mathbf{p}_{22}+6U_\infty^2\omega_1^2\mathbf{p}_{11}^2\mathbf{p}_{22}$$
$$+6\mathbf{p}_{12}^2\mathbf{p}_{22}\Big)$$

$$\gamma_8=-\mathbf{z}_2^{\mathrm{T}}\mathbf{Q}a_{311}$$
$$=-\frac{1}{N_{20}}\left(-\Lambda_2' c_s L_s-c_s T_s\right)(U_\infty^3\omega_1^3\mathbf{p}_{11}^3$$
$$+3U_\infty^2 b_0\omega_1^3\mathbf{p}_{11}^2\mathbf{p}_{12}-3b_0\omega_1\mathbf{p}_{12}^3+b_0^3\omega_1^3\mathbf{p}_{12}^3$$
$$-3U_\infty\omega_1\mathbf{p}_{12}^2\mathbf{p}_{11}+3U_\infty\omega_1^3 b_0^2\mathbf{p}_{12}^2\mathbf{p}_{11})$$

$$\gamma_9=\mathbf{z}_2^{\mathrm{T}}\mathbf{Q}a_{310}$$
$$=\frac{1}{N_{20}}\left(-\Lambda_2' c_s L_s-c_s T_s\right)$$
$$(3b_0^2\omega_1^2\mathbf{p}_{12}^3+6U_\infty b_0\omega_1^2\mathbf{p}_{12}^2\mathbf{p}_{11}$$
$$+3U_\infty^2\omega_1^2\mathbf{p}_{12}\mathbf{p}_{11}^2-\mathbf{p}_{12}^3)$$

References

1. Priya, S., Inman, D.J.: Energy Harvesting Technologies. Springer, New York (2009)
2. Wei, C., Jing, X.: A comprehensive review on vibration energy harvesting: modelling and realization. Renew. Sustain. Energy Rev. **74**, 1–18 (2017)
3. Huang, R., Hu, H.Y., Zhao, Y.H.: Designing active flutter suppression for high-dimensional aeroelastic systems involving a control delay. J. Fluids Struct. **34**, 33–50 (2012)
4. Huang, R., Hu, H.Y., Zhao, Y.H.: Single-input/single-output adaptive flutter suppression of a three-dimensional aeroelastic system. J. Guid. Control Dyn. **35**(2), 659–665 (2012)
5. Huang, R., Qian, W.M., Hu, H.Y., Zhao, Y.H.: Design of active flutter suppression and wind-tunnel tests of a wing model involving a control delay. J. Fluids Struct. **55**, 409–427 (2015)
6. Huang, R., Zhao, Y.H., Hu, H.Y.: Wind-tunnel tests for active flutter control and closed-loop flutter identification. AIAA J. **54**(7), 2089–2099 (2016)
7. Liu, H.J., Hu, H.Y., Zhao, Y.H., Huang, R.: Efficient reduced-order modeling of unsteady aerodynamics robust to flight parameter variations. J. Fluids Struct. **49**, 728–741 (2014)
8. Liu, H.J., Zhao, Y.H., Hu, H.Y.: Adaptive flutter suppression for a fighter wing via recurrent neural networks over a wide transonic range. Int. J. Aerosp. Eng. **2016**, 1–9 (2016)
9. Abdelkefi, A.: Aeroelastic energy harvesting: a review. Int. J. Eng. Sci. **100**, 112–135 (2016)
10. Li, D., Wu, Y., Da, Ronch A., et al.: Energy harvesting by means of flow-induced vibrations on aerospace vehicles. Prog. Aerosp. Sci. **86**, 28–62 (2016)
11. Zhao, L., Yang, Y.: Toward small-scale wind energy harvesting: design, enhancement, performance comparison, and applicability. Shock Vib. **2017**, 1–31 (2017)
12. Mehmood, A., Abdelkefi, A., Hajj, M.R., et al.: Piezoelectric energy harvesting from vortex-induced vibrations of circular cylinder. J. Sound Vib. **332**(19), 4656–4667 (2013)
13. Zhang, L.B., Abdelkefi, A., Dai, H.L., et al.: Design and experimental analysis of broadband energy harvesting from vortex-induced vibrations. J. Sound Vib. **408**, 210–219 (2017)
14. Barrero-Gil, A., Alonso, G., Sanz-Andres, A.: Energy harvesting from transverse galloping. J. Sound Vib. **329**(14), 2873–2883 (2010)
15. Yang, Y., Zhao, L., Tang, L.: Comparative study of tip cross-sections for efficient galloping energy harvesting. Appl. Phys. Lett. **102**(6), 064105 (2013)
16. Erturk, A., Vieira, W.G.R., De Marqui Jr., C., et al.: On the energy harvesting potential of piezoaeroelastic systems. Appl. Phys. Lett. **96**(18), 184103 (2010)
17. De Marqui, C., Vieira, W.G.R., Erturk, A., et al.: Modeling and analysis of piezoelectric energy harvesting from aeroelastic vibrations using the doublet-lattice method. J. Vib. Acoust. **133**(1), 011003 (2011)
18. Bryant, M., Garcia, E.: Modeling and testing of a novel aeroelastic flutter energy harvester. J. Vib. Acoust. **133**(1), 011010 (2011)
19. Abdelkefi, A., Nayfeh, A.H., Hajj, M.R.: Modeling and analysis of piezoaeroelastic energy harvesters. Nonlinear Dyn. **67**(2), 925–939 (2012)
20. Bibo, A., Daqaq, M.F.: Energy harvesting under combined aerodynamic and base excitations. J. Sound Vib. **332**(20), 5086–5102 (2013)
21. Bibo, A., Daqaq, M.F.: Investigation of concurrent energy harvesting from ambient vibrations and wind using a single piezoelectric generator. Appl. Phys. Lett. **102**(24), 243904 (2013)

22. Yan, Z., Abdelkefi, A.: Nonlinear characterization of concurrent energy harvesting from galloping and base excitations. Nonlinear Dyn. **77**(4), 1171–1189 (2014)
23. Dai, H.L., Abdelkefi, A., Wang, L.: Piezoelectric energy harvesting from concurrent vortex-induced vibrations and base excitations. Nonlinear Dyn. **77**(3), 967–981 (2014)
24. Zhao, L., Yang, Y.: An impact-based broadband aeroelastic energy harvester for concurrent wind and base vibration energy harvesting. Appl. Energy. **212**, 233–243 (2018)
25. Rocha, R.T., Balthazar, J.M., Tusset, A.M., et al.: Nonlinear piezoelectric vibration energy harvesting from a portal frame with two-to-one internal resonance. Meccanica. **52**(11–12), 2583–2602 (2017)
26. Chen, L.Q., Jiang, W.A., Panyam, M., et al.: A broadband internally resonant vibratory energy harvester. J. Vib. Acoust. **138**(6), 061007 (2016)
27. Xiong, L., Tang, L., Mace, B.R.: A comprehensive study of 2: 1 internal-resonance-based piezoelectric vibration energy harvesting. Nonlinear Dyn. **91**(3), 1817–1834 (2018)
28. Cao, D.X., Leadenham, S., Erturk, A.: Internal resonance for nonlinear vibration energy harvesting. Eur. Phys. J. Spec. Top. **224**(14–15), 2867–2880 (2015)
29. Yang, W., Towfighian, S.: Internal resonance and low frequency vibration energy harvesting. Smart Mater. Struct. **26**(9), 095008 (2017)
30. Gilliatt, H.C., Strganac, T.W., Kurdila, A.J.: An investigation of internal resonance in aeroelastic systems. Nonlinear Dyn. **31**(1), 1–22 (2003)
31. Chen, L.Q., Jiang, W.A.: Internal resonance energy harvesting. J. Appl. Mech-T. ASME. **82**(3), 031004 (2015)
32. Chen, L.Q., Jiang, W.A.: A piezoelectric energy harvester based on internal resonance. Acta Mech. Sin. **31**(2), 223–228 (2015)